Orientation Selectivity in Visual Cortex by Fluctuation-Controlled Criticality

Louis Tao[(1)], David Cai[(2)], David McLaughlin[(2,3)], Robert Shapley[(3)], and Michael Shelley[(2,3)]

[(1)] Department of Mathematical Sciences
New Jersey Institute of Technology
323 Martin Luther King, Jr., Blvd, Newark, NJ 07102

[(2)] Courant Institute of Mathematical Sciences
New York University
251 Mercer Street, New York, NY 10012

[(3)] Center for Neural Science
New York University
4 Washington Place, New York, NY 10003

CAMS Report 0405-27, Spring 2005

Center for Applied Mathematics and Statistics

NJIT

Orientation Selectivity in Visual Cortex by Fluctuation-Controlled Criticality

L. Tao[1], D. Cai[2], D. McLaughlin[2,3], R. Shapley[3], and M. Shelley[2,3]

[1]Department of Mathematical Sciences, NJIT

Newark, NJ 07102

[2]Courant Institute of Mathematical Sciences &

[3]Center for Neural Science

New York University, New York, NY 10012

Abstract. We examine how synaptic fluctuations modify the effects of strong recurrent network amplification to produce orientation selectivity in a large-scale neuronal network model of the macaque primary visual cortex. Previously, we showed that the model reproduces many of the experimentally observed properties of simple and complex cells, through a balance between feedforward and recurrent excitation. However, strong cortical amplification leads to network instabilities, unrealistically high firing rates and complex cells that are not orientation selective, even in the presence of strong cortical inhibition. In this paper, we show that large fluctuations in the cortico-cortical conductances can stabilize the network, allowing strong cortical gain and the emergence of orientation selective complex cells. By increasing the strength of synaptic fluctuations, say, through sparsifying the network connectivity, we identify a transition between two types of dynamics, mean- and fluctuation-driven. In a network with strong recurrent excitation, this fluctuation-controlled transition is signified by a near hysteretic behavior and a rapid rise of network firing rates as the synaptic drive or stimulus input is increased. We discuss the connection between this transition and orientation selectivity in our model of primary visual cortex.

1 Introduction

Orientation selectivity and spatial summation are two of the most fundamental visual processing tasks performed by the mammalian primary visual cortex (V1). V1 is the first area along the visual pathway where neurons are selective for stimulus orientation. Individual neurons in V1 respond preferentially to lines and edges of a particular orientation. This orientation selectivity is also independent of stimulus contrast: In measurements of orientation tuning curves, e.g., firing rates of individual neurons as a function of stimulus orientation, the bandwidth (half-width at half maximum), the circular variance (CV), and the orientation selectivity index of individual tuning curves are roughly independent of stimulus contrast. Furthermore, based on spatial summation properties, V1 neurons are classified as "simple" or "complex". Simple cells respond to visual stimulation in an approximately linear fashion, while complex cells respond nonlinearly. For example, when driven by drifting sinusoidal gratings, a simple cell follows the temporal modulation of the drifting grating as the grating moves across the receptive field of the neuron, whereas complex cells show an elevated and unmodulated response. Quantitatively, simple and complex cellular responses is often differentiated by the modulation ratio F1/F0 (the ratio of the first Fourier component and the mean) of the cycle-averaged firing rate [1]: cells with $F1/F0 > 1$ are simple and cells with $F1/F0 < 1$ are complex.

How orientation selectivity arises in V1 has not been fully elucidated [2, 3]. According to the classical Hubel and Wiesel picture, orientation selectivity directly arises from the convergence of lateral geniculate (LGN) afferents [4]. However, modelling based on the Hubel and Wiesel, or "feedforward," picture shows that the degree of selectivity provided by the convergent LGN inputs alone is insufficient to explain extant data [2]. Some form of cortical processing appears necessary. Furthermore, in purely feedforward models, at higher contrasts broader tuning is expected since the feedforward drive surpasses threshold at more orientations. (This is the so-called iceberg effect.) Noise in the membrane potential has been

suggested to be important for contrast invariance [5, 6, 7, 8]. How this "noise" arises in the visual cortical network is yet to be understood.

Modifications of the feedforward scheme use Hebbian ideas to posit cortical circuitry with highly specific cortical inhibition. The push-pull model is an example of such a modification: intracortical inhibition is anti-correlated with the excitatory synaptic drive [9]. However, other models, without highly feature specific coupling, demonstrate that selectivity can arise from the sharpening of weakly tuned feedforward excitation by broadly tuned intracortical inhibition (see, e.g., [10, 11, 12]). The so-called marginal phase arises when cortical excitation is sufficiently strong to allow symmetry-breaking states [13].

Previously we studied how simple and complex cellular responses arise in a large-scale neuronal network model of an input layer $4C\alpha$ of macaque V1 [14]. The model represents a 1 mm^2 local patch with 4 orientation hypercolumns containing $\sim O(10^4)$ conductance based, integrate-and-fire (I&F) neurons — 75% excitatory and 25% inhibitory. The cortical architecture, the LGN drive, and the cortico-cortical synaptic couplings are constrained whenever possible by anatomical and physiological measurements [15, 16, 14]. In this large-scale model, a continuum of simple and complex cellular responses arise from the varying degrees of balance between cortico-cortical and feedforward inputs: the most "simple" of the model neurons are driven strongly by the LGN and are "linearized" by strong cortical inhibition [16], while the most "complex" receive strong cortical excitation and inhibition [14]. This particular model, while it reproduces many aspects of simple and complex cell bahavior, does not have complex cells that are orientation selective. The strong cortical amplification causes an apparent bistability: complex cells tend to fire at rates that are too high (and are limited by the absolute refractory period) or not at all. Reasonable complex cell firing rates can be obtained after the introduction of sufficiently strong noise. In [17], we suggested that strong cortical fluctuations may stabilize network dynamics and allow complex cell selectivity. In this paper, within the framework of a simplified version of [14],

we demonstrate how strong synaptic fluctuations in sparsely-coupled networks or networks with synaptic failure, can transform potentially destabilizing recurrent network amplification to near-bistability in a regime dominated by fluctuations. In simple cells, strong dynamic synaptic fluctuations provide the "noise" to circumvent the iceberg effect. In complex cells, the near bistability provides rapid, graded response to recurrent amplification for contrast-invariant orientation selectivity. We further elucidate these mechanisms in so-called "ring models" and examine the role of V1 architecture on orientation selectivity. Finally, the role of synaptic fluctuations is analyzed detail using the bifurcation phase diagrams of an all-to-all network model.

2 Methods

Our systems of conductance-based I&F neurons, whose individual **membrane potentials** $v_P^j(t)$ follow

$$\frac{dv_P^j}{dt} = -g_L\ \left(v_P^j - V_R\right) - g_{PE}^j(t)\ \left(v_P^j - V_E\right) - g_{PI}^j(t)\left(v_P^j - V_I\right), \quad P = E, I. \tag{1}$$

The m^{th} spike time, t_m^j, of the j^{th} model neuron, is determined by $v_P^j(t_m^{j-}) = V_T$; $v_P^j(t_m^j + \tau_{ref}) = V_R$, where τ_{ref} is an absolute refractory period. Here the membrane potentials of the excitatory (E) (inhibitory (I)) neurons are denoted by v_E^j (v_I^j), where the superscript j indexes the spatial location of the neuron within the network. g_L, g_{PE}, and g_{PI} are the leak, excitatory, and inhibitory conductances, respectively. We use normalized, dimensionless potentials with $V_I = -2/3, V_T = 1, V_R = 0$, and $V_E = 14/3$ [15]. We take $\tau_{ref} = 3$ ms (1 ms) for excitatory (inhibitory) neurons.

In this work, we introduce a simplification of large-scale model of [14]: The **time-dependent conductances** arise from the input forcing (through the LGN), from the cortical network activity of the excitatory and inhibitory populations, and have the general form

$$g_{PE}^j(t) \;\; = \;\; F_{PE}(t) + [(1-\lambda^j)S_{PE} + S_{PE}^0] \sum_k a_{j,k} \sum_l p_{kl}^j G_E(t - t_l^k),$$

$$g_{PI}^{j}(t) \;=\; F_{PI}(t) + S_{PI}\sum_{k} b_{j,k}\sum_{l} p_{kl}^{j} G_I(t-t_l^k), \tag{2}$$

where $F_{PE}(t) = \lambda^j g_{lgn}^j(t)$ (the conductance $g_{lgn}^j(t)$ denotes the feedforward forcing from the LGN), $F_{PI}(t) = c_{inh}\sum_i G_I\left(t-s_l^j\right)$ is a stimulus-independent inhibition modeled by homogeneous Poisson spike trains. The kernels $a_{j,k}$ and $b_{j,k}$ describe the spatial structure of the cortical coupling and are normalized to have unit sum so that the S_{PE} and S_{PI}'s denote synaptic strengths. We take $S_{EI} = S_{II}$ so that the cortical inhibition is the same for both excitatory and inhibitory neurons. The parameter $\lambda^j \in [0,1]$ in these equations indicates heuristically how the distribution of simple and complex cells is set in our models and characterizes the simple-complex nature of the j^{th} neuron (with $\lambda^j = 0$ the most complex, $\lambda^j = 1$ the most simple, and S_{PE}^0 models weak cortical excitatory couplings for simple cells), by setting the strength of LGN drive relative to the strength of the cortico-cortical excitation. The parameter λ^j is distributed uniformly in $[0,1]$ for our large-scale V1 model.

The postsynaptic conductances (PSC) $G_{E/I}(t-t_l^k)$ are $\Theta(t-t_l^k)\,(\tau_d-\tau_r)^{-1}\left[\exp\left(\frac{-(t-t_l^k)}{\tau_d}\right) - \exp\left(\frac{-(t-t_l^k)}{\tau_r}\right)\right.$ where Θ is the Heaviside function. The time constants are $\tau_r = 1, 2, 1$ ms and $\tau_d = 5, 80, 10$ ms for AMPA, NMDA and $GABA_A$, respectively. For excitatory synapses, $G_E(t-t_l^k) = (1-f_N)\,G_{AMPA}(t-t_l^k) + f_N G_N(t-t_l^k)$, where f_N denotes the fractional contribution of NMDA receptors. For networks with synaptic failure p_{kl}^j is a Bernoulli random variable chosen to be 1 with probability p for each spike-time; for *sparse* networks, p_{kl}^j is independent of l, is chosen to be 1 with probability p and is fixed for individual realizations of the network model. Thus, in both types of networks, each neuron is coupled to $N_{eff} = pN$ other presynaptic neurons statistically.

Each model is closed by the specification of network architecture. The first model is a simplified version of the model of [14]. The cortical architecture, LGN drive and cortico-cortical couplings, is described in detail in [15, 16, 14][1]. To examine the effects of synaptic

[1] In the model we study here, we do not model feedback from other layers and extrastriate areas, which was modeled as activity-dependent feedback in [14], we do not consider the second, longer inhibitory synaptic timecourse, and we set the synaptic coupling parameters to be fixed constants instead of being Gaussian distributed. Long-range inhibitory effects are modeled as an all-to-all inhibitory coupling: In the results

fluctuations, we study networks with the same synaptic coupling parameters, but vary the strength of a single postsynaptic conductance by synaptic failure or by network sparsity (p_{kl}^{j}). For instance, the mean and the variance of a single excitatory PSC induced in an excitatory cell scale as $1/N_{eff}$.

To isolate the effect of synaptic fluctuation dynamics on amplification and orientation tuning, we also study a series of "ring model," whose neurons are labeled by their orientation preference, θ^j, and are coupled to each other by $a_{j,k} = A\left(\theta^j - \theta^k\right)$, where A is a Gaussian kernel, with the excitatory lengthscale twice that of inhibition ($\sigma_e = 2\sigma_i$). The parameter λ^j is either 0 or 1: Half the neurons receive no LGN excitation but strong cortico-cortical excitation. The other half of the neurons receive weak cortico-cortical excitation and strong LGN excitation, taken as Gabor functions and parameterized by preferred orientation θ^j and preferred spatial phase φ^j. Under drifting gratings, the convergent LGN drive is modeled as in [6]: $F_{EE}(t) = F_{IE}(t) = g_{lgn}^{j}(t) = c_0 \sum_l G\left(t - s_l^j\right)$, where the l^{th} "spike-time" received by the j^{th} neuron is given by a Poisson process with time-dependent rate $\nu_{LGN}^{j}(\theta, t) = d_0\left(1 + \frac{1}{2}\varepsilon\left(1 + \cos 2\left(\theta - \theta^j\right)\right)\sin\left(\frac{2\pi}{\omega}t - \varphi^j\right)\right)$, where $\varepsilon, \theta, \omega$ are stimulus contrast, orientation and temporal frequency, respectively. Note that the mean LGN input is independent of stimulus orientation but the temporal modulations are largest for $\theta = \theta^j$, i.e., the preferred orientation.

Finally, we use bifurcation phase diagrams to accentuate the effects of synaptic fluctuations in an all-to-all network network without spatial structure ($a_{j,k} = 1/N_{eff}$). $F_{EE}(t) = F_{IE}(t) = g_{lgn}^{j}(t) = c_0 \sum_l G\left(t - s_l^j\right)$, for $j = 1, ..., N/2$. Here the l^{th} "spike-time" received by the j^{th} neuron is given by a homogeneous Poisson process with rate ν_{LGN}.

shown in Figs. 1-3, $b_{j,k} = (1/2) \times (b_{j,k}^{0} + 1/N_{eff}))$, where $b_{j,k}^{0}$ is Gaussian in the distance between neurons j and k and is normalized to unity.

3 Results

3.1 Orientation Selectivity in a Large-Scale Model of V1

Orientation selectivity is measured using orientation tuning curve, i.e., time-average firing rates as a function of stimulus orientation. A tuned neuron responds strongly at a few orientations and shows very little response at the "orthogonal" orientation. In our large-scale model, both simple and complex cells show orientation selective responses. Figure 1 shows the tuning properties of two neurons: an excitatory simple (ES) cell near a pinwheel singularity and a excitatory complex (EC) cell far from any pinwheel centers. (Under drifting grating stimulation, cells with F1/F0 ¿ 1 are simple, cells with F1/F0 ¡ 1 are complex.) The simple cell (top panels) is strongly driven by the LGN, whereas the complex cell (bottom panels) is not driven by the LGN. These cells have firing rates that are contrast invariant: their CVs are nearly equal at high and low contrasts (solid and dashed lines, respectively, in Figs. 1a and 1c). Figs. 1b and 1d show the synaptic conductances as functions of stimulus orientation at high contrast: mean plus one standard deviation of the LGN drive (its time-average under drifting grating is independent of orientation), and time-averages of the (excitatory and inhibitory) cortico-cortical conductances. The tuning of the simple cell comes from the modulating component of the LGN drive. Near pinwheel centers, the cortical conductances come from a population of cells with broadly distributed preferred orientations and are therefore nearly independent of stimulus orientation. As one moves from a pinwheel center into an iso-orientation domain, the synaptic coupling is between cells with nearly the same preferred orientation, leading to orientation selective cortical conductances (Fig. 1d). Model complex cells become selective as its tuned excitatory conductance overcomes its tuned inhibitory conductance.

Figure 2 summarizes the tuning properties of the excitatory neurons in this model. Fig. 2a shows the distribution of CV for the ES and the EC population separately. Both populations are broadly distributed in CV (with ES cells better tuned than EC cells), in qualitatively

agreement with experimental data [18]. Fig. 2b indicates that the orientation selectivity is approximately contrast invariant: the CV at high stimulus contrast is roughly equal to the CV at low stimulus contrast (even though the data shows a large scatter).

In producing these model results, large regions of the synaptic coupling strength parameter space were explored. We find that in order to have contrast invariant orientation selective complex cells, there must be strong recurrent excitation [14] with large temporal fluctuations [17]. To understand the effect of synaptic fluctuations on network dynamics, we systematically varied N_{eff}, through synaptic failure or through network sparsity. (Figures in this section displayed results from a network with synaptic failure, but qualitatively similar results were reproduced in sparsely coupled networks.)

Without sufficient synaptic fluctuations, the complex cells tended to be bistable in the presence of the strong recurrent excitation needed for cortical amplification and for orientation tuning. This can be illustrated by comparing model networks with different N_{eff}. Fixing the stimulus (drifting grating) orientation (say, at θ_0), the stimulus contrast was increased from zero contrast to 100% contrast before it was decreased to zero. Let ΔN_{spikes} denote the difference in the number of spikes during the contrast decrement and during the contrast increment. Figure 3 shows the distribution of ΔN_{spikes} of the excitatory simple and the excitatory complex population for networks with different N_{eff}. For the network model with $N_{eff} = 96$ ($N_e = 72$ and $N_i = 24$), the neurons are not hysteretic: the distribution of ΔN_{spike} is symmetric about 0. In the network with larger N_{eff} ($= 768$), the distribution of ΔN_{spikes} for the excitatory complex population is skewed: the complex cells are hysteretic in stimulus contrast. Note that this hysteresis increases as N_{eff} is further increased.

A distinct feature of this large-scale model is the spatial distribution of selectivity relative to the location of pinwheel centers. As shown in Fig. 2c, the ES cells are better tuned near pinwheel centers and the EC cells are better tuned in iso-orientation domains. How this arises from the interaction of strongly fluctuating recurrent coupling with the cortical architecture

can be unveiled in the analysis of two simpler models. As we show next, analysis of the so-called "ring" models reveals the mechanisms that underlie the spatial distribution. How synaptic fluctuations transform the relation between synaptic inputs and neuronal outputs will be examined in section 3.3 with an all-to-all model.

3.2 Orientation Selectivity in Ring Models

We examine "ring models" consisting of neurons at a fixed distance from a pinwheel center. To study the spatial distribution in selectivity, we construct a series of rings, ranging from small rings at or near pinwheel centers ("near rings") to larger rings away from any pinwheel singularity ("far rings"). The isotropic and homogeneous cortico-cortical couplings in our V1 model is mapped onto near and far ring models by varying the coupling lengthscales in the ring models from $\sigma_e = \sigma_i = \infty$ to $\sigma_e = 0.16$ and $\sigma_i = 0.08$ rads ($\sim$ 200 μm and 100 μm in a ring of radius 0.25 mm). We further idealize by considering only two populations: $\lambda^j = 1$ for $j = 1, \ldots, N/2$ and $\lambda^j = 0$ for $j = N/2 + 1, \ldots, N$. We have numerically simulated models with and without all-to-all (global) cortico-cortical inhibition. The results we describe below are from models without global cortico-cortical inhibition [2].

The spatial distribution of CV in our V1 model can be reproduced in a series "ring models," with fixed synaptic coupling strengths but different σ_e and σ_i (keeping $\sigma_e = 2\sigma_i$). Figure 4 displays model ES and EC cell firing rate tuning curves in 4 rings. In the smallest ring, the cortical coupling is effectively all-to-all, thus the cortico-cortical inhibition is broadly tuned in orientation, leading to the most sharply tuned simple cell. Figure 4b shows that as we move away from the pinwheel center, the inhibition becomes more tuned. The main effect of the tuned inhibition is to detune the simple cell.

Figure 4e shows that cortico-cortical excitation follow the same trend as inhibition as we move away from the pinwheel center. Thus near the pinwheel center, a complex cell receiving untuned excitation will not be orientation selective at all. However, in the $\sigma_e = 0.16$ ring,

[2] Stimulus-independent inhibition was used instead.

cortico-cortical excitation can be sharply tuned, leading to sharply tuned complex cells. Note that excitatory couplings have to be sufficiently strong to overcome the detuning effects of tuned inhibition in the far ring.

The orientation selectivity is also contrast invariant. Figure 5 shows the tuning curves of 4 model neurons (Fig. 5a: near ES, b: far ES, c: near EC, d: far EC) at 4 stimulus contrast ($\epsilon = 0.25, 0.5, 0.75, 1$). The orientation tuning curves of each cell are roughly scaled versions of each other as we change stimulus contrast (although there is a plateau in the turning curve of the near ring simple cell).

As we found in our V1 model, strong recurrent excitation with large fluctuations is necessary to reproduce contrast-invariant orientation selective complex cells. Without sufficiently strong synaptic fluctuations, the ring model networks are also bistable. Figure 6 displays the tuning curves for EC cells at different contrasts for 3 different NMDA/AMPA ratios $f_N = 0.225, 0.25, 0.275$ for a far ring model. (Note the results in Figs. 5 and 6 are from a $f_N = 0.25$ network.) For the $f_N = 0.225$ network, the EC cell is still roughly contrast invariant but is less tuned than the EC cell in the $f_N = 0.25$ network at each contrast. However, as we increase f_N above $f_N = 0.25$, even with merely 2.5% more NMDA, the network is bistable: at the highest contrast, the complex cell spike at a rate limited by the absolute refractory period. The same qualitative features of this transition are observed when N_{eff} is varied while f_N is fixed: at $N_{eff} = 96$, the EC cells are slightly less amplified and less tuned, at at $N_{eff} = 104$, the network is bistable at high contrasts (data not shown). The critical contrast at which the bistability occurs is lower for even larger networks.

A striking feature of this bistability is the sharpness of this transition in parameter space, even in the presence of large synaptic fluctuations. Within a few percent changes of f_N and N_{eff}, the far ring network dynamics varies from smoothly amplifying to bistable. This transition is less sharp in ring models with smaller radii (i.e., nearer to pinwheel center). Thus the network gain is influenced by the structure of the cortical architecture. To isolate

the effect of fluctuations, we turn next to an all-to-all model and examine how synaptic fluctuations transform the input-output relation of strongly recurrent networks.

3.3 Fluctuation-Controlled Criticality

Our all-to-all model consists of 50% neurons receiving feedforward drive (mimicking simple cells) and 50% neurons receiving strong intracortical excitation (mimicking complex cells). (Both populations receive the same, strong, cortico-cortical inhibition.) We ignore the detailed time-dependence of the visual drive, and focus instead on the dynamics of networks containing two types of cells (simple or complex: strongly driven by feedforward or by recurrent excitation) in the presence of synaptic fluctuations. Figure 7 displays the complex cell population firing rate as a function of the mean feedforward drive, $g_{Input} = c_0 \nu_{LGN}$, in networks with the same synaptic coupling strengths but of different N_{eff}. These firing rate curves are obtained by first increasing and then decreasing in succession the feedforward input. In the $N_{eff} = 200$ network, hysteresis is observed as we ramp up and then down the strength of the feedforward drive. This behavior is well-captured by the solution of our kinetic theory analysis (not shown) [17]. The transition is a saddle-node bifurcation in g_{Input} for the mean population firing rate. As N_{eff} is decreased (here by increasing the probability of synaptic failure, $1-p$), while strengthening individual synapses to keep the effective network drive constant, the region of bistable behavior in g_{Input} becomes smaller and smaller, until the bistability disappears completely and a smooth firing rate curve is observed (e.g., the curve for $N_{eff} = 25$).

The transition also occurs when we change the relative contributions of fast and slow excitation. NMDA receptors acts on a longer timescale and each PSC has a smaller temporal variance than a PSC mediated by AMPA receptors. Figure 8 displays the complex cell population firing rate as a function of g_{Input} in networks of fixed $N_{eff} = 25$ with different f_N ratios. Again, the firing rate curves are obtained by increasing and decreasing g_{Input}. In the case with no AMPA, hysteresis is observed and the dynamics is mean-driven. In the

case with no NMDA, there is no hysteresis and the dynamics is fluctuation-driven. While the results in Figs. 7 and 8 were computed in networks with synaptic failure (i.e., $p < 1$), these results hold in sparsely coupled networks, where individual neurons are postsynaptic targets for a set of randomly chosen but fixed number of neurons (N_{eff}).

To further illustrate the notion of fluctuation-driven dynamics, we rewrite the I&F equations as $\frac{dv^j}{dt} = -g_T(t)\left[v^j - V_S^j(t)\right]$, where g_T is the total conductance and V_S^j is an effective reversal potential, which is necessarily greater than the voltage threshold V_T whenever the neuron fires. In the statistically steady state situation, what distinguishes the bifurcation is the time-average of V_S^j. We say the dynamics is *mean-driven* whenever $\overline{V_S^j} = T^{-1}\int_{t_0}^{t_0+T} V_S^j(t)\,dt$ is greater than V_T, i.e., the mean of the synaptic input is sufficient to drive the neuron to fire. We call the other case *fluctuation-driven*, since temporal fluctuations in the drive are needed for spiking. This notion of fluctuation-driven dynamics is distinct from the dynamics of the so-called "balanced networks" where the overall excitatory and inhibitory currents nearly cancel [19, 20]. (In network models of Sects. 3.1 and 3.2, the mean synaptic currents are strongly inhibitory and the effective reversal potentials are far below threshold.)

The synaptic fluctuations have the effect of smoothing the relation between synaptic input and neuronal output in the form of spikes. With sufficiently strong recurrent excitation, as we increase the strength of synaptic fluctuations, the region of bistability in synaptic input shrinks to achieve near-hysteresis at a critical level of fluctuations. As we increase fluctuations even further, network is no longer hysteretic, but the network gain is decreased. Since this transition occurs as the amount of synaptic fluctuations is varied, we call it **fluctuation-controlled criticality**. The network dynamics near this point is characterized by near-bistability and rapid changing firing rates as a function of synaptic input.

4 Discussion

The emerging picture of the cortical network shows a state dominated by fluctuations [21, 5, 22]. While much work has focused in the smoothing effect of these fluctuations, in this paper, we have unveil a fluctuation-driven bifurcation, whose distinguishing behavior includes a rapid change in rates as a function of synaptic drive and near hysteresis. The sharp transition near this point can be revealed by adjusting the amount of synaptic fluctuations, by changing N_{eff} via synaptic failure or network sparsity, or by changing f_N, the relative contributions of AMPA and NMDA. As we decreased fluctuations, the network gain is increased until a critical level, after which the network becomes bistable. We have demonstrated that this mechanism underlies the dynamics and tuning of a ring model, containing contrast invariant orientation selective neurons: stronger fluctuations lead to weaker network gain and less orientation selectivity; weaker fluctuations leads to stronger network gain and network bistability.

This signatures of fluctuation-driven criticality are also seen in our large-scale model of V1. Changing $N_{eff} = 96$ to $N_{eff} = 768$ moves the network from a fluctuation-driven to a mean-driven regime. In the network with larger N_{eff}, the complex cells become hysteretic when we ramp up and down stimulus contrast. (We note that in two-population versions of this model, this transition is much sharper, as it is in the two population ring models.) In the mean-driven network, the complex cells tend to be bistable, fire at rates that are too high and are not orientation selective. Our analysis suggests that pharmacological manipulations of the cortical network can change its operating point. We can move a mean-driven, hysteretic state towards the critical state by decreasing f_N, the relative contributions of fast and slow excitations. Similarly, we can move a fluctuation-dominated, non-selective network towards the critical state by increasing f_N. Although the N_{eff} and f_N of the V1 cortical network is not known, our work suggests that the network operates near a fluctuation-controlled critical state and that selective complex cells are found away from pinwheel centers.

In our V1 and our ring models, we incorporated either a global component in the cortico-cortical inhibition (in our V1 and our ring models — ring model data not shown) or a

stimulus-independent inhibitory component (ring model results shown.) The origin of a global inhibition is yet to be understood. In V1, although the lengthscale of monosynaptic local inhibition is half that of local excitation, there is strong evidence for an effectively global inhibition [23, 24]. This global inhibition can be provided by disynaptic inhibition [25, 26] within each V1 layer or by intralaminar or extrastriate connections (refs).

In our models, near complex cells and far simple cells tend to be less orientation selective. Near pinwheel centers, both excitatory and inhibitory synaptic conductances are nearly independent of orientation. Thus a near complex cell will have flat tuning curves in both membrane potential and firing rates. In iso-orientation domains, inhibition is shorter ranged than feedforward excitation. Thus a far simple cell will be less orientation selective than a near simple cell. Recent works of M. Sur and his colleagues show that on averages, pinwheel center cells and iso-orientation domain cells tend to have similiar tuning in the firing rates, even though the tuning of the average membrane potential is sharper away from pinwheels. It may be necessary to incorporate longer ranged, inter-hypercolumn or intralaminar couplings to explain these features, and will be taken up in future work.

How contrast invariant orientation selectivity arises in V1 is one of the important problems of visual neuroscience [2, 3]. An immediate problem confronting any model is that the Hubel-Wiesel thalamo-cortical drive is broader at high contrasts, as the input at non-preferred orientations becomes super-threshold. Some form of noise is often invoked to provide contrast invariance in simple cells. Assuming that a transfer function between membrane potential and neuronal firing rates can be found, [7, 8] showed that a power transfer function is the only relation that transforms contrast invariant membrane potential tuning curves to contrast invariant spike responses. Within a wide range of contrasts, stimulus-independent noise does transform threshold-linear firing rate curves into approximate power laws in the membrane potential [27, 7, 8] consistent with experimental findings [5]. However, the effects of synaptic conductances has not been considered and how contrast invariant membrane

potentials arise in the first place is not yet understood. Here we show that synaptic fluctuations provides a natural form of "noise," allowing the iceberg effect to be circumvented in simple cells, while the fluctuation-controlled criticality gives rise to contrast-invariant orientation-selective V1 complex cells.

While many of our model results can be analyzed using kinetic theory and population density equations [17], here we have given a mechanistic account of how contrast invariance may be achieved in a fluctuation-driven setting, and relegate the theoretical analysis to a forthcoming note. Here we have demonstrated that an important effect of synaptic fluctuations is to stabilize network dynamics in highly recurrent networks so that large cortical gain is possible at a fluctuation-controlled critical point, which is the mechanism that underlies contrast invariance in a model of the V1 cortical network.

Acknowledgement D.C. is supported by Sloan Fellowship and by NSF Grants DMS-0211655 and DMS-9729992. D.W.M is supported by NSF Grant DMS-0211655.

References

[1] B. C. Skottun, R. L. De Valois., D. H. Grosof, J. A. Movshon, D. G. Albrecht, and A. B. Bonds. Classifying simple and complex cells on the basis of response modulation. *Vision Res*, 31(7-8):1079–1086, 1991.

[2] H. Sompolinsky and R. Shapley. New perspectives on the mechanisms for orientation selectivity. *Curr. Opin. Neurobiol.*, 7:514–522, 1997.

[3] D. Ferster and K. D. Miller. Neural mechanisms of orientation selectivity in the visual cortex. *Annu Rev Neurosci*, 23:441–471, 2000.

[4] D. Hubel and T. Wiesel. Receptive fields and functional architecture of the monkey striate cortex. *J. Physiol. (Lond)*, 195:215–243, 1968.

[5] J. Anderson, I. Lampl, D. Gillespie, and D. Ferster. The contribution of noise to contrast invariance of orientation tuning in cat visual cortex. *Science*, 290:1968–1972, 2000.

[6] M. Shelley and D. McLaughlin. Coarse-grained reduction and analysis of a network model of cortical response. I. drifting grating stimuli. *submitted*, 2002.

[7] K. Miller and T. Troyer. Neural noise can explain expansive, power-law nonlinearities in neural response functions. *J. Neurophysiol.*, 87:653–659, 2002.

[8] D. Hansel and C. van Vreeswijk. How noise contributes to contrast invariance of orientation tuning in cat visual cortex. *J. Neurosci.*, 22:5118–5128, 2002.

[9] T. Troyer, A. Krukowski, N. Priebe, and K. Miller. Contrast invariant orientation tuning in cat visual cortex with feedforward tuning and correlation based intracortical connectivity. *J. Neurosci.*, 18:5908–5927, 1998.

[10] D. Somers, S. Nelson, and M. Sur. An emergent model of orientation selectivity in cat visual cortical simple cells. *J. Neurosci.*, 15:5448–5465, 1995.

[11] M. Carandini and D. L. Ringach. Predictions of a recurrent model of orientation selectivity. *Vision Res*, 37(21):3061–3071, Nov 1997.

[12] P. Adorjan, J. Levitt, J. Lund, and K. Obermayer. A model for the intracortical origin of orientation preference and tuning in macaque striate cortex. *Vis. Neurosci.*, 16:303–318, 1999.

[13] R. Ben-Yishai, R. Bar-Or, and H. Sompolinsky. Theory of orientation tuning in the visual cortex. *Proc. Nat. Acad. Sci. USA*, 92:3844–3848, 1995.

[14] L. Tao, M. Shelley, D. McLaughlin, and R. Shapley. An egalitarian network model for the emergence of simple and complex cells in visual cortex. *Proc. Natl. Acad. Sci. USA*, 000:000–000, 2004.

[15] D. McLaughlin, R. Shapley, M. Shelley, and J. Wielaard. A neuronal network model of macaque primary visual cortex (V1): Orientation selectivity and dynamics in the input layer $4C\alpha$. *Proc. Natl. Acad. Sci. USA*, 97:8087–8092, 2000.

[16] J. Wielaard, M. Shelley, R. Shapley, and D. McLaughlin. How Simple cells are made in a nonlinear network model of the visual cortex. *J. Neurosci.*, 21(14), 2001.

[17] D. Cai, L. Tao, M. Shelley, and D. McLaughlin. A new kinetic representation of fluctuation-driven neuronal networks with application to simple & complex cells in primary visual cortex. *Proc. Natl. Acad. Sci. USA*.

[18] D. Ringach, R. Shapley, and M. Hawken. Orientation selectivity in macaque V1: Diversity and laminar dependence. *J. Neurosci.*, 22(13):5639–5651, 2002.

[19] C. van Vreeswijk. and H. Sompolinsky. Chaos in neuronal networks with balanced excitatory and inhibitory activity. *Science*, 274(5293):1724–1726, Dec 1996.

[20] C. van Vreeswijk. and H. Sompolinsky. Chaotic balanced state in a model of cortical circuits. *Neural Comput*, 10(6):1321–1371, Aug 1998.

[21] M. N. Shadlen and W. T. Newsome. The variable discharge of cortical neurons: implications for connectivity, computation, and information coding. *J Neurosci*, 18(10):3870–3896, May 1998.

[22] M. Rudolphe and A. Destexhe. Characterization of subthreshold voltage fluctuations in neuronal membranes. *Neural Comp.*, 15:2577–2618, 2003.

[23] D. Ringach, M. Hawken, and R. Shapley. Dynamics of orientation tuning in macaque primary visual cortex. *Nature*, 387:281–284, 1997.

[24] D. Ringach, M. Hawken, and R. Shapley. Dynamics of orientation tuning in macaque V1: The role of global and tuned suppression. *J. Neurophysiol.*, 90:342–352, 2003.

[25] D.J. Pinto and G.B. Ermentrout. Spatially structured activity in synaptically coupled neuronal networks: II. lateral inhibition and standing pulses. *SIAM J. Appl. Math.*, 62:226–243, 2001.

[26] K. Kang, M.J. Shelley, and H. Sompolinsky. Mexican hats and pinwheels in visual cortex. *Proc. Natl. Acad. Sci. USA*, 100:2848–2853, 2003.

[27] M. Carandini and D. Ferster. Membrane Potential and Firing Rate in Cat Primary Visual Cortex. *J. Neurosci.*, 20:470–484, 2000.

5 Figure Captions

Figure 1: Two sample cells from V1 model. a)-b) Orientation tuning curves for an excitatory Simple cell: a) Firing Rate (high contrast, solid; low contrast, dashed), b) Conductances (at high contrast) (F1 component of LGN, dashed; cortical excitation, solid; cortical inhibition, dotted). c)-d) corresponding figures for an excitatory Complex cell. The synaptic coupling parameters are $S_{ee} = 0.0$, $S_{ie} = 6.0$ for the simple cells; $S_{ee} = 4.9$, $S_{ie} = 6.5$ for the complex cells; $S_{ei} = S_{ii} = 2.0$ for all cells. $N_{eff} = 64$ and the AMPA/NMDA ratio is $f_N = 0.25$.

Figure 2: Orientation Selectivity of Excitatory Cells in V1 model: a) Histogram of CV for excitatory Simple cells (top) and excitatory Complex cells (bottom); b) CV of excitatory cells at high and low contrasts; c) CV, mean and standard deviation, of ES (solid) and EC (dashed) cells as a function of distance to nearest pinwheel center.

Figure 3: Hysteresis in V1 Model. The distribution in ΔN_{spike} (the difference in spikes during ramp-up and ramp-down of stimulus contrast) for the excitatory simple (dashed) and excitatory complex (solid lines) populations: a) $N_{eff} = 96$, b) $N_{eff} = 768$. The model parameters are the same as in Fig. 1. The complex cells of the $N_{eff} = 768$ network tend to be hysteretic in stimulus contrast.

Figure 4: Orientation Selectivity of Ring Models. a)-c) Tuning curves for firing rate, LGN drive, and cortical inhibitory for an excitatory simple cell in 4 rings. In a) and c), the firing rate and the inhibitory conductances are show for 4 rings — solid: $\sigma_e = 2.0$; dotted: $\sigma_e = 0.5$; dash-dotted: $\sigma_e = 0.25$; dashed: $\sigma_e = 0.16$. b) the mean and standard deviation of the LGN conductance — solid: mean LGN drive; dashed: plus and minus one standard deviation. d)-f) Tuning curves for firing rate, cortical excitation, and cortical inhibition for an excitatory complex cell in the same 4 rings. The model parameters are $S_{ee} = 0.0$, $S_{ie} = 7.5$, $C_{ee} = 9.5$, $C_{ie} = 8.0$, $S_{ei} = S_{ii} = C_{ei} = C_{ii} = 2.0$; $N_{eff} = 100$; $f_N = 0.25$.

Figure 5: Contrast Invariance in Ring Models. Firing rate uning curves for four cells at

four contrast ($\varepsilon = 0.25, 0.5, 0.75, 1.0$): a) ES cell in near ring, b) ES cell in far ring, c) EC in near ring, d) EC cell in far ring. Near ring model parameters as in Fig. 4 with $\sigma_e = \infty$, $\sigma_i = \infty$. Far ring model parameters as in Fig. 4 with $\sigma_e = 0.16$, $\sigma_i = 0.08$.

Figure 6: Hysteresis in Far Ring Model. Firing rate tuning curving (at four contrasts) for 3 network with different f_N: a) $f_N = 22.5\%$, b) $f_N = 25\%$, and c) $f_N = 27.5\%$. The network model with the largest f_N is hysteretic: at the strongest stimulus contrast, the complex cell population firing rate is limited by the absolute refractory period.

Figure 7: Firing rate *vs.* G_{Input} curves for four networks with different $N_{eff} = 25$, 50, 100, and 200. These curves were obtained by first increasing and then decreasing the strength of the feedforward excitation G_{Input}. The network synaptic coupling strengths are $S_{ee} = S_{ie} = 0.25$ for the simple Cell population; $S_{ee} = S_{ie} = 0.5$ for the complex Cell population; and $S_{ei} = S_{ii} = 0.9$ for all cells. $f_N = 0.0$ for all models shown.

Figure 8: Firing rate *vs.* G_{Input} curves for four networks with different $f_N = 0$, 25%, 50%, 75%, and 100%. These curves were obtained by first increasing and then decreasing the strength of the feedforward excitation G_{Input}. The network synaptic coupling strengths are the same as in Fig. 5. $N_{eff} = 25$ for all models shown.

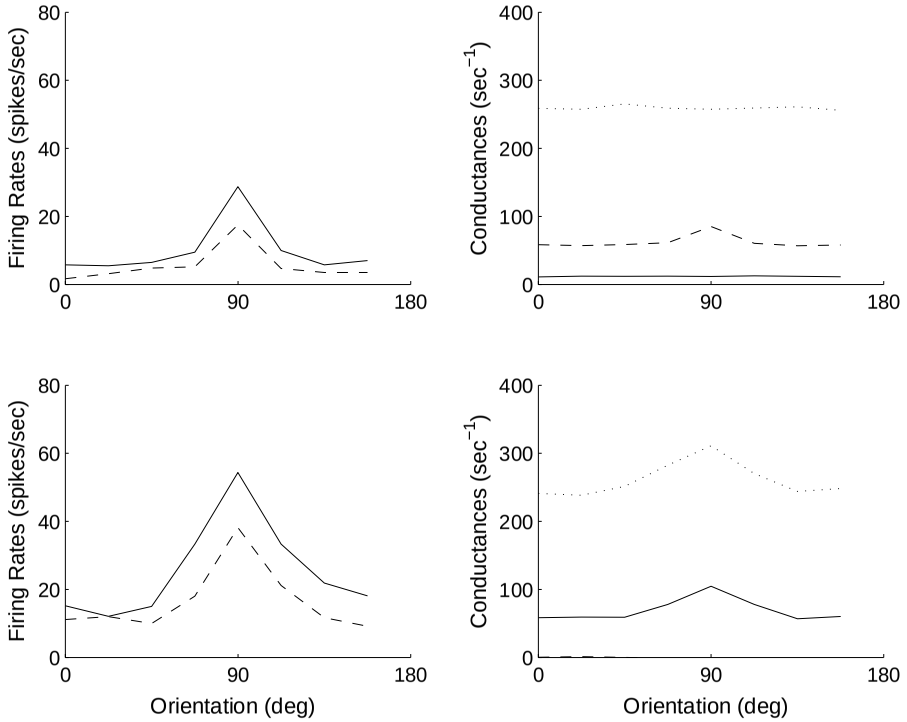

Figure 1: Two sample cells from V1 model. a)-b) Orientation tuning curves for an excitatory Simple cell: a) Firing Rate (high contrast, solid; low contrast, dashed), b) Conductances (at high contrast) (F1 component of LGN, dashed; cortical excitation, solid; cortical inhibition, dotted). c)-d) corresponding figures for an excitatory Complex cell. The synaptic coupling parameters are $S_{ee} = 0.0$, $S_{ie} = 6.0$ for the simple cells; $S_{ee} = 4.9$, $S_{ie} = 6.5$ for the complex cells; $S_{ei} = S_{ii} = 2.0$ for all cells. $N_{eff} = 64$ and the AMPA/NMDA ratio is $f_N = 0.25$.

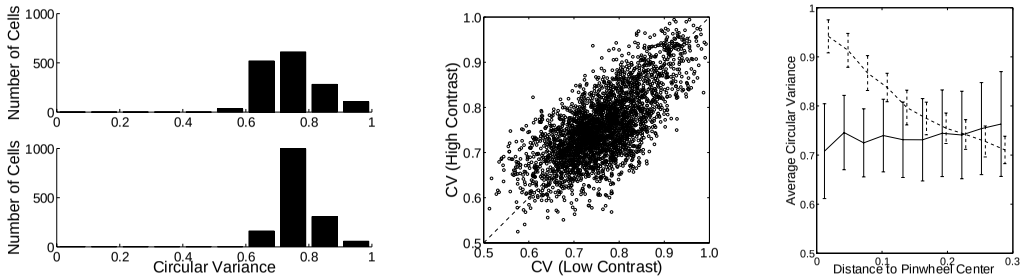

Figure 2: Orientation Selectivity of Excitatory Cells in V1 model: a) Histogram of CV for excitatory Simple cells (top) and excitatory Complex cells (bottom); b) CV of excitatory cells at high and low contrasts; c) CV, mean and standard deviation, of ES (solid) and EC (dashed) cells as a function of distance to nearest pinwheel center.

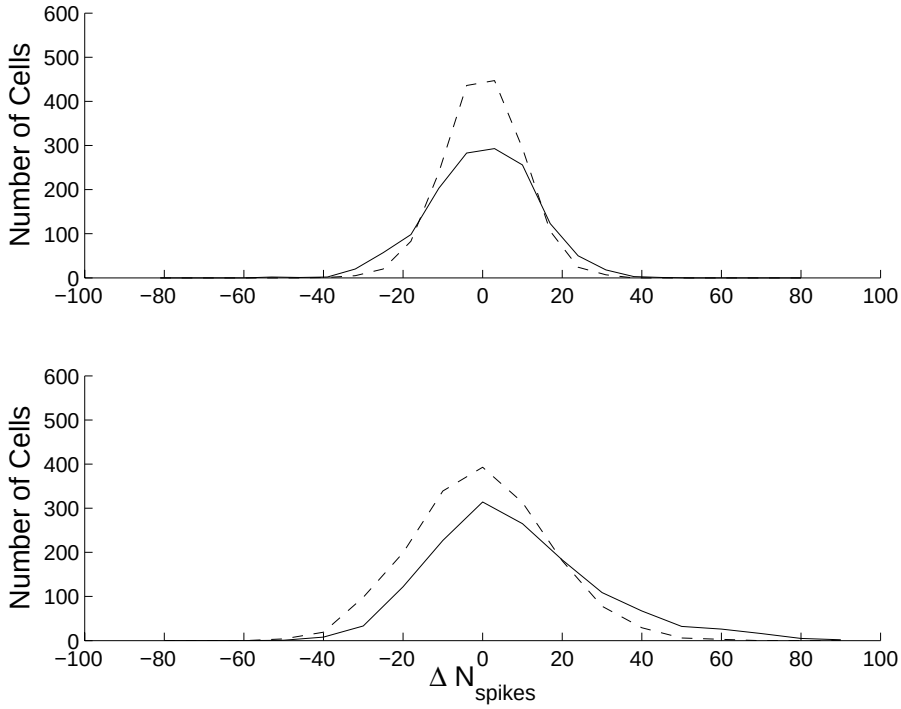

Figure 3: Hysteresis in V1 Model. The distribution in ΔN_{spike} (the difference in spikes during ramp-up and ramp-down of stimulus contrast) for the excitatory simple (dashed) and excitatory complex (solid lines) populations: a) $N_{eff} = 96$, b) $N_{eff} = 768$. The model parameters are the same as in Fig. 1. The complex cells of the $N_{eff} = 768$ network tend to be hysteretic in stimulus contrast.

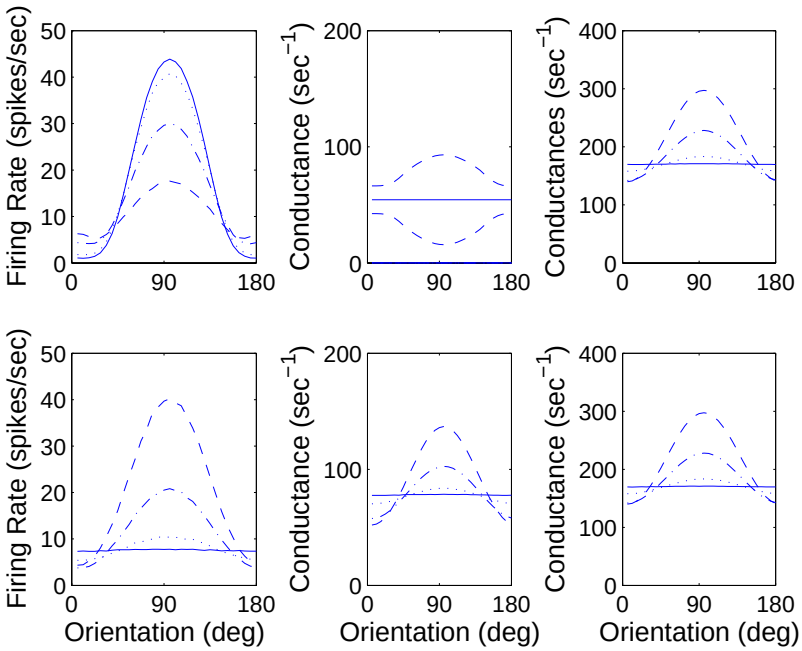

Figure 4: Orientation Selectivity of Ring Models. a)-c) Tuning curves for firing rate, LGN drive, and cortical inhibitory for an excitatory simple cell in 4 rings. In a) and c), the firing rate and the inhibitory conductances are show for 4 rings — solid: $\sigma_e = 2.0$; dotted: $\sigma_e = 0.5$; dash-dotted: $\sigma_e = 0.25$; dashed: $\sigma_e = 0.16$. b) the mean and standard deviation of the LGN conductance — solid: mean LGN drive; dashed: plus and minus one standard deviation. d)-f) Tuning curves for firing rate, cortical excitation, and cortical inhibition for an excitatory complex cell in the same 4 rings. The model parameters are $S_{ee} = 0.0$, $S_{ie} = 7.5$, $C_{ee} = 9.5$, $C_{ie} = 8.0$, $S_{ei} = S_{ii} = C_{ei} = C_{ii} = 2.0$; $N_{eff} = 100$; $f_N = 0.25$.

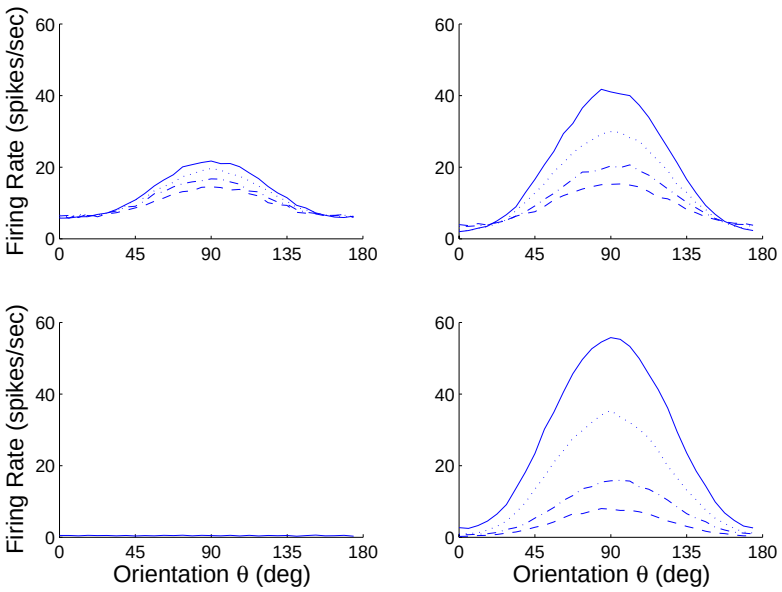

Figure 5: Contrast Invariance in Ring Models. Firing rate uning curves for four cells at four contrast ($\varepsilon = 0.25, 0.5, 0.75, 1.0$): a) ES cell in near ring, b) ES cell in far ring, c) EC in near ring, d) EC cell in far ring. Near ring model parameters as in Fig. 4 with $\sigma_e = \infty$, $\sigma_i = \infty$. Far ring model parameters as in Fig. 4 with $\sigma_e = 0.16$, $\sigma_i = 0.08$.

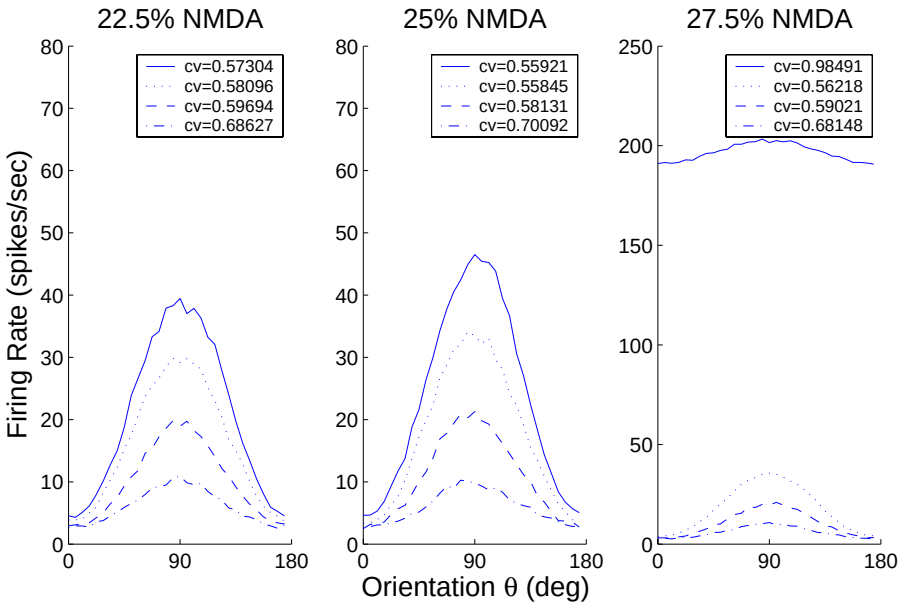

Figure 6: Hysteresis in Far Ring Model. Firing rate tuning curving (at four contrasts) for 3 network with different f_N: a) $f_N = 22.5\%$, b) $f_N = 25\%$, and c) $f_N = 27.5\%$. The network model with the largest f_N is hysteretic: at the strongest stimulus contrast, the complex cell population firing rate is limited by the absolute refractory period.

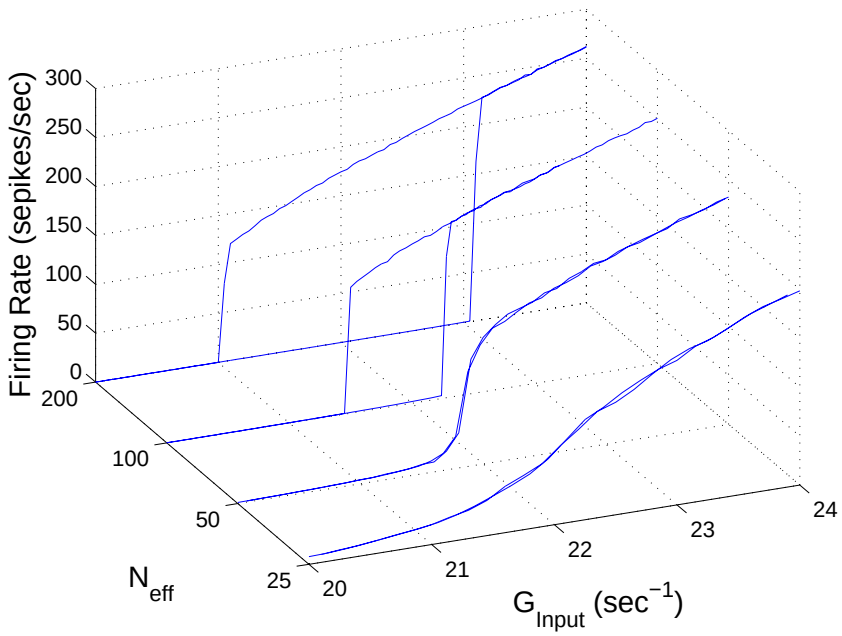

Figure 7: Firing rate *vs.* G_{Input} curves for four networks with different $N_{eff} = 25$, 50, 100, and 200. These curves were obtained by first increasing and then decreasing the strength of the feedforward excitation G_{Input}. The network synaptic coupling strengths are $S_{ee} = S_{ie} = 0.25$ for the simple Cell population; $S_{ee} = S_{ie} = 0.5$ for the complex Cell population; and $S_{ei} = S_{ii} = 0.9$ for all cells. $f_N = 0.0$ for all models shown.

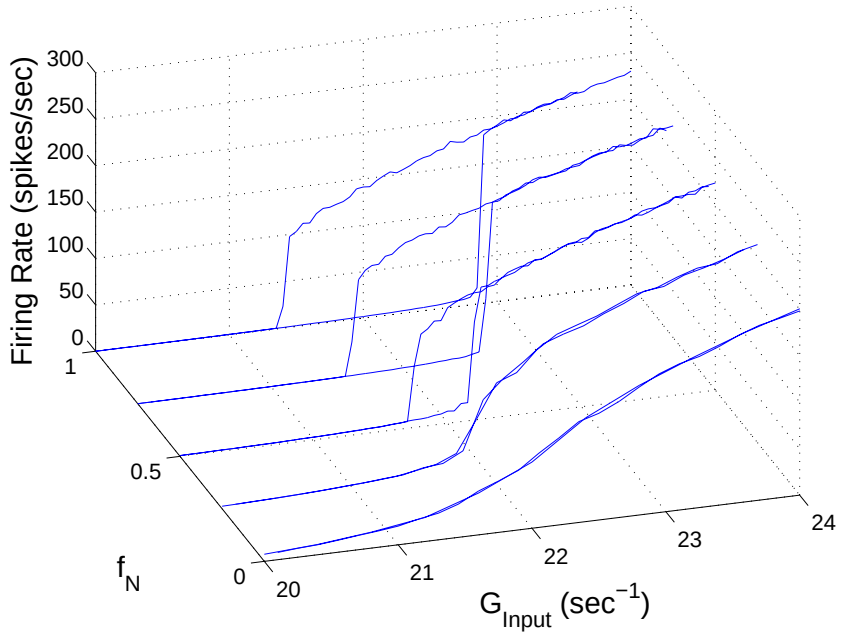

Figure 8: Firing rate *vs.* G_{Input} curves for four networks with different $f_N = 0$, 25%, 50%, 75%, and 100%. These curves were obtained by first increasing and then decreasing the strength of the feedforward excitation G_{Input}. The network synaptic coupling strengths are the same as in Fig. 5. $N_{eff} = 25$ for all models shown.